Chapter 1 Introduction

Weathering of minerals is an important geologic process that plays a significant role in much of the geochemistry of the earth's surface, ranging from rock erosion rates to seawater chemistry. Laboratory dissolution studies are an important step in deriving models to help interpret environmental weathering. These studies help in the understanding of, e.g., metal cation release in soils, regulation of atmospheric CO_2, groundwater chemistry, and clay formation.

Investigators have inferred the existence of a leached layer on feldspar and wollastonite surfaces because of the discrepancy in the cation release when conducting dissolution experiments (Bailey and Reesman, 1971; Chou and Wollast, 1984). These leached layers are important for numerous reasons: leached layers may act as substrates for new mineral formation (Banfield & Barker, 1994; Banfield et al., 1995); leached layers may play a significant role in increasing BET surface areas reported in laboratory studies (Stillings and Brantley, 1995) and in field studies (White et al., 1996); the leached layers may restructure into something resembling vitreous silica (Casey et al., 1993) and produce an ever increasing barrier to the release of the more soluble components of the mineral.

Wollastonite was chosen for this dissolution study because it is a fast reacting mineral, it has a simple structure similar to chain silicates, it has a simple composition, ($CaSiO_3$), there is availability of pure material, and it reportedly forms a leached layer (Bailey and Reesman, 1971; Casey et al., 1993; Xie and Walther, 1994;). The goal of this study was to gain a better understanding of why leached layers form on dissolving wollastonite and how these layers influence the dissolution process. This paper presents the results of a series of dissolution experiments where operating conditions were varied in an effort to discover their affect on the development of the leached layer of wollastonite. BET surface areas were measured for a majority of the samples and leached layer thickness was calculated where possible. Most of the experiments were performed in a newly designed external recycle mixed-flow reactor that held the material fixed, yet thoroughly mixed material and solution.

Chapter 2 Materials

The wollastonite used in this study is the same material that was used by Rimstidt and Dove (1986). This wollastonite was mined in New Mexico, USA, and was obtained from Wards Scientific Establishment. The material was hand sorted to remove macroscopic impurities and then crushed in a steel mortar. The crushed wollastonite was dry-sieved to recover the 75-150 μm and 150-250 μm size grains. The fractions were then immersed in alcohol and manually agitated for 5 minutes. The cloudy supernatant was decanted and replaced with fresh alcohol. This process was repeated 3 to 5 times until the supernatant was relatively clear. The wollastonite was then rinsed with distilled, deionized H_2O for 5 minutes and dried overnight in an oven at 75^{o} C. The samples were placed in capped glass containers and stored under air until use. Scanning electron microscopic (SEM) examination of the unreacted wollastonite revealed a few fine particles still adhering to the

surface (Fig. 1a). The bulk composition of the unreacted material was verified by energy dispersive X-ray (EDX) analysis of individual particles (Appendix B). The initial surface area of the 150-250 μm size fraction was determined by a 3-point N_2 BET to be 0.302 $\pm$ 0.045 $m^2 g^{-1}$. Run solutions were prepared with reagent grade concentrated nitric acid and calcium nitrate.

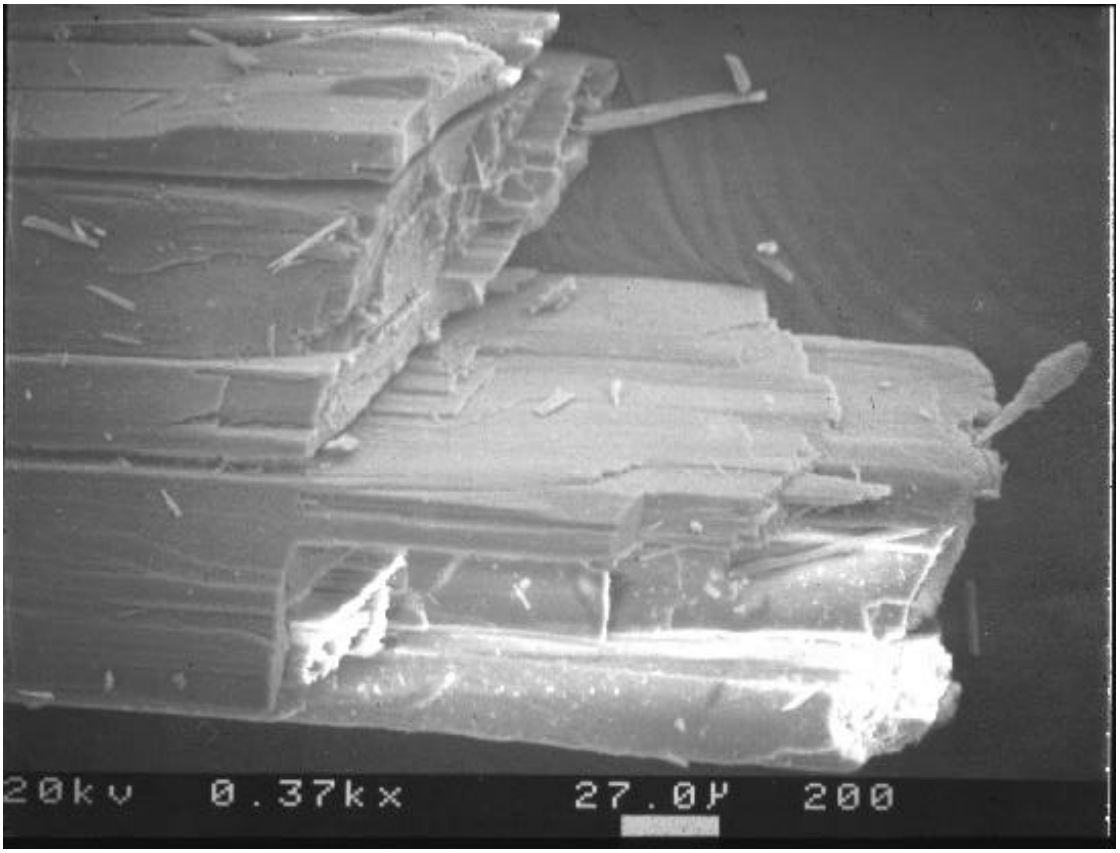

FIG. 1a. SEM photograph of unreacted wollastonite after washing and rinsing with alcohol. Though very fine particles are adhering to the surface, they do not contribute to final dissolution rates as they are quickly reacted away (See Fig. 1b).

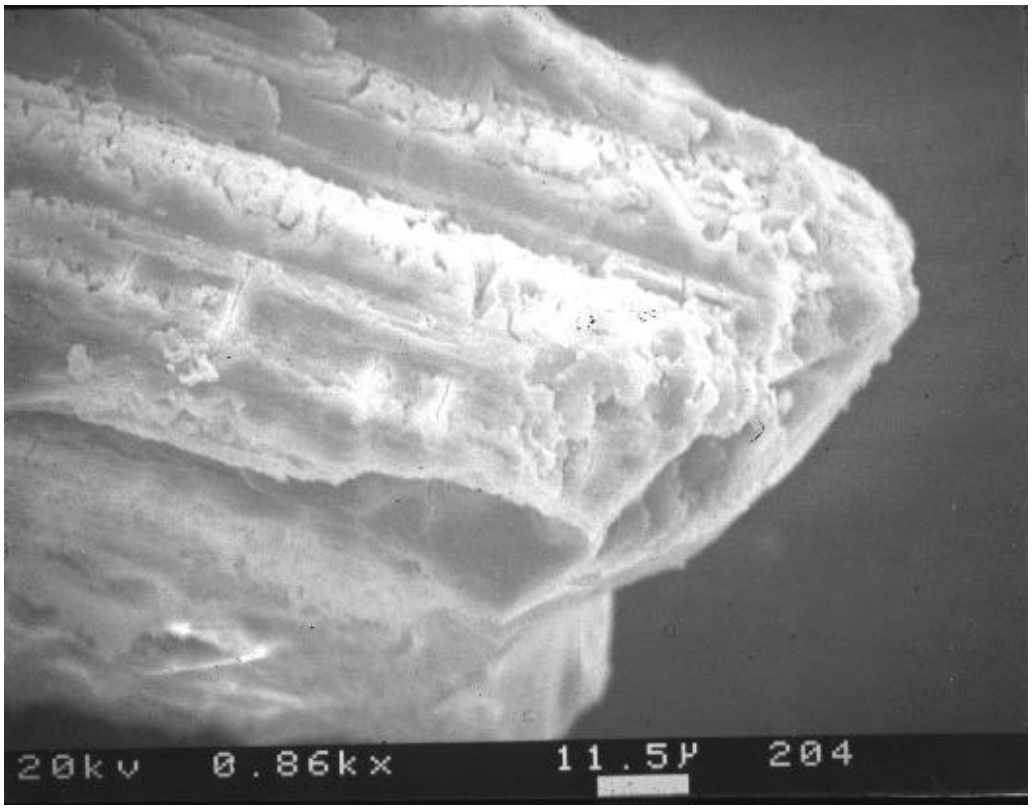

FIG. 1b. SEM photograph of wollastonite reacted for 190 hours at pH 2 in a mixed flow reactor. Though the sample has been degraded by mechanical mixing, the dehydrated Si-enriched leached layer is still visible.

Chapter 3 Reactor Design

Preliminary experiments using a mixed flow reactor stirred by means of a suspended magnetic stir bar showed that the wollastonite dissolution reaction is transport-limited at slow stirring rates. This behavior was determined by varying stirring rates and noting the increasing release rates with increasing stirring speed. When stirring rates were increased sufficiently to overcome the transport-limited behavior, the stir bar caused comminution of the grains. In order to overcome this problem, a fixed-bed external recycle mixed flow reactor was designed and constructed. This design (Fig. 2) was used for the majority of the experiments. This new reactor produced a high enough mixing rate to eliminate a transport limited reaction without the comminution produced by mechanical stirring. The reactor can operate with various amounts of solid, however 1 gram proved sufficient for the experiments in this study.

A schematic diagram of the overall system is shown in Fig. 3 and an engineering drawing of the reactor is shown in Appendix C. The reactor was machined from a solid Acrylic® rod. The O-rings were made of Buna-n and the 70 µm nylon mesh was cemented to the O-rings with a styrene-based adhesive. The total volume of the reactor plus circulation loop was 47.00 $\pm$ 0.01 mL with approximately 1 gram of wollastonite loaded in the

reactor. The circulation loop consisted of 1/4" ID clear Tygon® tubing. The recycle flow used to mix the system (r_c) was provided by a high volume peristaltic pump. The recycle flow rate was varied by experiment to ensure that reaction rates were not transport limited. Feed solution was provided from a 25 L reservoir.

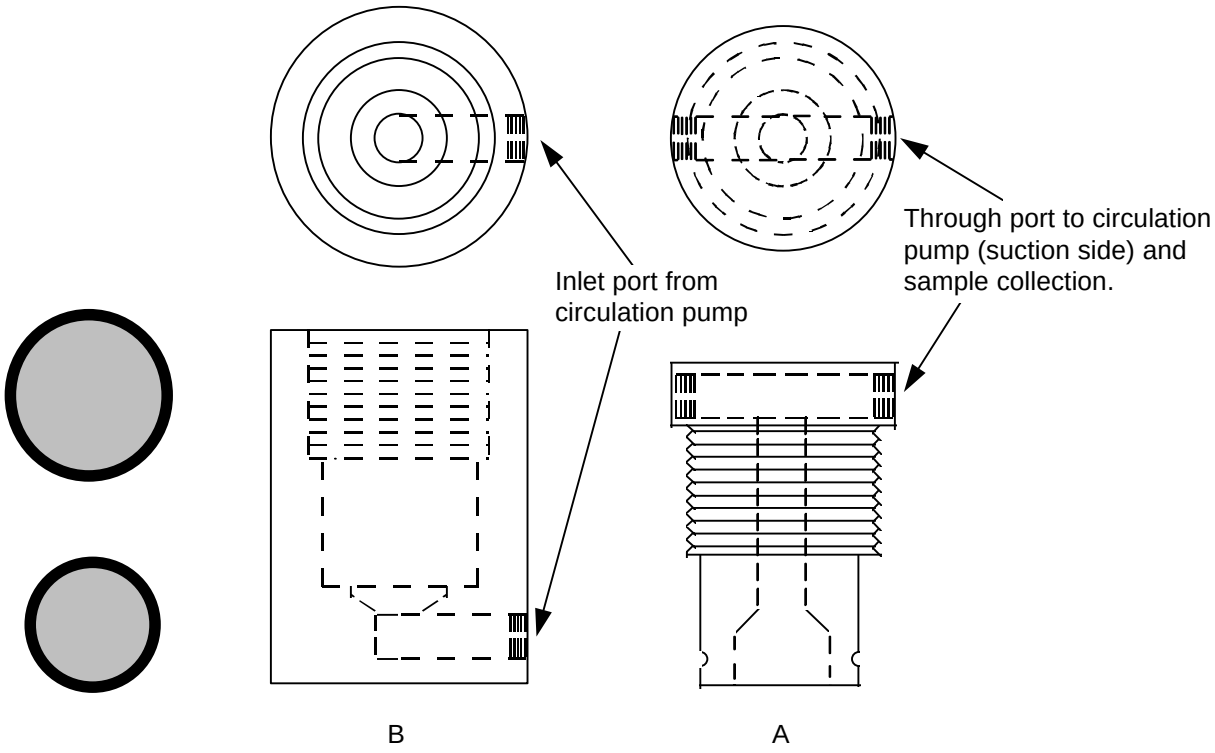

FIG. 2. Schematic representation of the Fixed bed external recycle mixed flow reactor. The material is placed into the small O-ring assembly which is inserted into the large O-ring assembly. This fixed bed of material is then inserted into "B" and held in place by the assembly of "A" into "B". A detailed version of this drawing is in Appendix C.

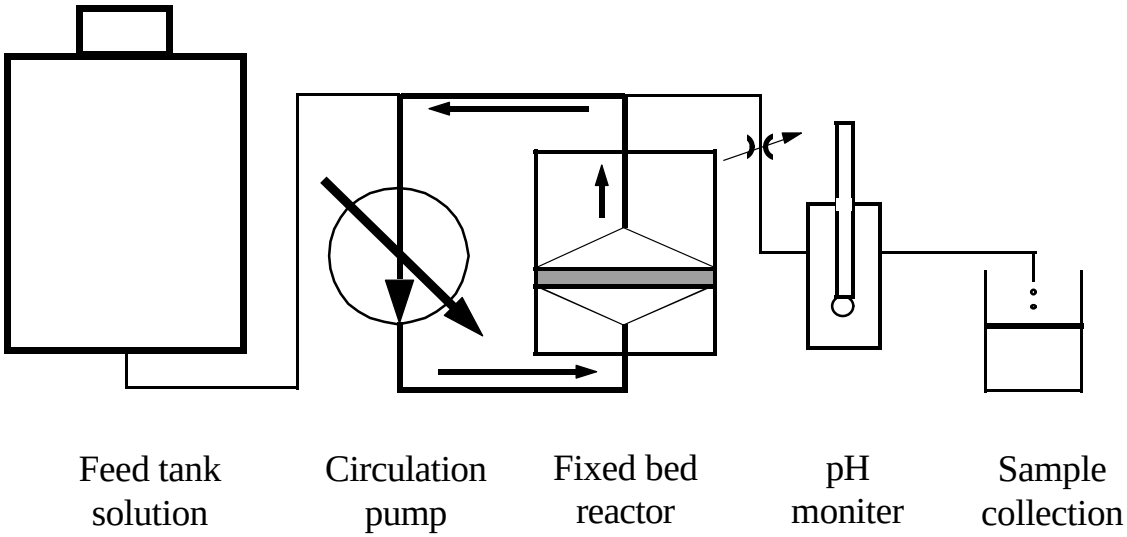

FIG. 3. Schematic diagram representing the experimental setup used in this study. The circulation pump supplied the pressure needed to circulate as well as feed the solution. The arrows trace the circulation loop through the material. Feed was regulated by a flow control valve placed in the line before sample collection.

Chapter 4 Experimental Protocol

Experiments were begun by loading approximately 1 g of 150-250 μm wollastonite into the small mesh covered O-ring and inserting it into the large mesh covered O-ring (Fig. 2). This fixed bed of wollastonite was then inserted into the reactor and the two halves screwed snugly together. The reactor was then connected to the circulation loop and submerged in a 25^{o} C constant temperature water bath. The 25 L feed solution tank was filled with solution, the stopcock opened, air bled from the system, and recycling begun. Flow (r_f) through the experiment was immediately adjusted to the desired rate by the use of a tubing clamp. This effluent flow rate that determined the residence time in the reactor was varied from experiment to experiment to test the effects of varying residence time.

Release rate curves were compared for the first four experiments and it was found that after 14 hours the Ca and Si release rates had reached an apparent steady state. The rates continued to decrease after 14 hours, but from 14 to 96 hours, the length of the longest experiment, the Si release rate decreased only 0.3 log units. The experimental protocol then became to run all dissolution experiments for approximately 24 hours and compare the release rates from 14 to 24 hours, however some longer experiments were conducted.

The peristaltic circulating pump was operated at settings from 4.5 to 10. These settings corresponded to recycle rates through the material (r_c) of 0.70 to 1.40 L min^{-1} (Darcy velocities of 0.041 - 0.082 m/s). The recycle rate was measured at the end of experiments by removing the return tubing from the top of the reactor, plugging the tubing, and collecting a sample from the reactor for 20 to 30 sec in a 1.0 L beaker. The collected

sample was then weighed and recycle rate calculated as the quotient of the mass/time. The transport limited condition was checked by running the experiment with a constant flow rate and only varying the recycle rate. It was found that the calculated dissolution rates were comparable for recycle flow rates greater than 0.70 L min^{-1}. Flow rates were varied from < 0.0001 L min^{-1} to > 0.0015 L min^{-1}. The flow rate was measured by collecting a 30 mL sample for a period of time from 2 to 15 min, weighing the sample, and then calculating the rate.

At the conclusion of an experiment the reacted wollastonite was removed from the reactor and rinsed with distilled, deionized water and dried in an oven at 75° C for 30 minutes.

Chapter 5 Analytic Methods

Solution samples, typically 30 mL, were collected at various intervals during the experiments into polyethylene bottles Samples with pH ≥ 3 were acidified with 1.0 mL 0.6 N nitric acid to prevent cations from adsorbing to the sample bottles. The pH of the effluent was monitored continuously with an electrode calibrated at pH 4.01 and pH 7.00 using Fisher brand standards. Si concentrations were determined by the molybdate blue colorimetric procedure using Fisher brand Si standards (APHA, 1985). Ca concentrations were determined by Atomic Adsorption Spectroscopy using Fisher brand Ca standards. Surface area measurements were performed on samples outgassed under a vacuum at 300°C for 3 to 24 hours in a Quantachrome Nova 1000 Surface Area Analyzer. After degassing, the surface area was then calculated from a 3-point BET N_2 adsorption isotherm (Brunauer et al., 1938). SEM images were taken with a ISI - SX 40 operated with an accelerating voltage of 20kV. Qualitative standardless compositional analyses (EDX) were collected using a Noran Micro-Z Series energy dispersive spectrometer.

Chapter 6 Results

Table 1 is a compilation of all runs and operating conditions. Terms used in Table 1 and throughout this thesis are defined in Appendix A. Normalized release rates (r_j) for Si and Ca from wollastonite were calculated using the following equation (Rimstidt and Newcomb, 1992) from the average final cation concentrations in the effluent:

$$r_j = \frac{m_j \cdot r_f}{A_{sp} \cdot M} \qquad (1)$$

The release rates of Si and Ca calculated for each experiment were normalized using initial surface areas (A_{sp}) are shown in Table 1. The total error associated with r_j was determined to be <10% based on an error analysis of the variables measured. Because the uncertainties used in the calculation are assumed to be independent and random, the total error was calculated by the quadratic sum method (Taylor, 1982). All errors were determined from analyzing the same sample three times. The precision of the Si analysis was found to be ±11% and the precision of the Ca analysis was ±10%. The error associated with the flow rate is ±0.03%. The precision of the specific surface area is ±15%.

Table 1. Compilation of experimental run conditions and the resulting dissolution rates calculated from initial specific surface area.

Run	Mixing Rate	Final pH	Initial/final mass (g)	Run time (hrs)	Flow rate (mL sec^{-1})	r_{Si} (mol m^{-2} s^{-1})	r_{Ca} (mol m^{-2} s^{-1})
A*	stirred	2.03	1.00/NA	191.1	0.015	0.55×10^{-9}	4.79×10^{-9}
B*	stirred	4.67	1.00/0.87	214.1	0.017	1.89×10^{-9}	3.40×10^{-9}
D	10	5.90	1.00/1.00	25.2	0.019	1.66×10^{-9}	6.01×10^{-9}
G	10	4.00	0.79/0.77	7.0	0.235	2.82×10^{-9}	13.5×10^{-9}
G.1	7	3.80	1.01/0.98	24.5	0.163	1.66×10^{-9}	10.0×10^{-9}
H	5	3.91	1.05/0.98	25.0	0.283	2.58×10^{-9}	12.2×10^{-9}
I	5	4.00	1.03/0.97	26.2	0.095	1.66×10^{-9}	8.21×10^{-9}
J	10	2.90	1.03/1.00	24.9	0.191	1.49×10^{-9}	11.8×10^{-9}
S	5	2.90	1.04/1.00	25.0	0.169	1.62×10^{-9}	6.76×10^{-9}
K	10	2.90	1.02/0.96	25.4	0.091	1.02×10^{-9}	7.79×10^{-9}
L	5	2.90	1.02/1.00	23.8	0.116	1.14×10^{-9}	8.12×10^{-9}
Hr	5	2.90	1.03/0.96	69.3	0.058 - 0.085	1.15×10^{-9}	8.03×10^{-9}
M"	10	5.90	1.02/1.01	25.0	0.210	0.54×10^{-9}	5.74×10^{-9}
N	4.5	5.90	1.01/0.97	24.5	0.220	2.20×10^{-9}	6.14×10^{-9}
P	10	5.96	1.04/1.00	24.3	0.239	1.89×10^{-9}	9.38×10^{-9}
Q	10	1.95	1.00/0.92	24.4	0.197	2.05×10^{-9}	10.5×10^{-9}
R	5	1.95	1.02/0.92	24.6	0.181	2.10×10^{-9}	8.89×10^{-9}
T	5	1.90	1.03/0.89	24.8	0.143	1.93×10^{-9}	NA
U	5	1.90	1.03/0.81	96.0	0.011 - 0.267	1.13×10^{-9}	7.82×10^{-9}

* Grain size reduction occurred during these experiments. These data were not used in subsequent data analysis.

" Potential problems with Si analysis. These data were not used in subsequent data analysis.

NA Data not available.

All of the experiments were run using 150 -250 μm wollastonite. Problems with Si analyses make the results of run M questionable, therefore it was not included in any of the data analysis. The first two experiments, A and B, were run using a mixed flow reactor with a suspended magnetic stir bar. Despite mixing speeds slow enough not to lift the material from the bottom of the reactor, the material was abraded into smaller size grains and the results were not used in the data analysis.

In all experiments, wollastonite dissolution was incongruent; Ca was always released at a higher rate than Si (Fig. 4). Figure 5 is representative of the typical Si and Ca dissolution rate over time for experiments run with flow rates >0.019 mL sec^{-1}. In contrast, at lower

flow rates Si release would slowly increase and asymptotically approach the Ca release from below. Because of the desire to maintain similar experimental conditions, experiments run with flow rates ≤ 0.019 mL sec^{-1} were avoided because of the 1 to 3 order of magnitude pH change when using pH solutions higher than 2.

Only initial release rates were affected by varying r_c and r_f. Figures 6 and 7 for experiments run at pH 3 demonstrate how the initial release rates of Si and Ca vary widely, but the final release rates are equal. Higher r_c and r_f produced higher initial release rates. This initial transport limited reaction could not be avoided with the laboratory equipment available for this investigation, however it is the final rates which are reported as the dissolution rate of wollastonite.

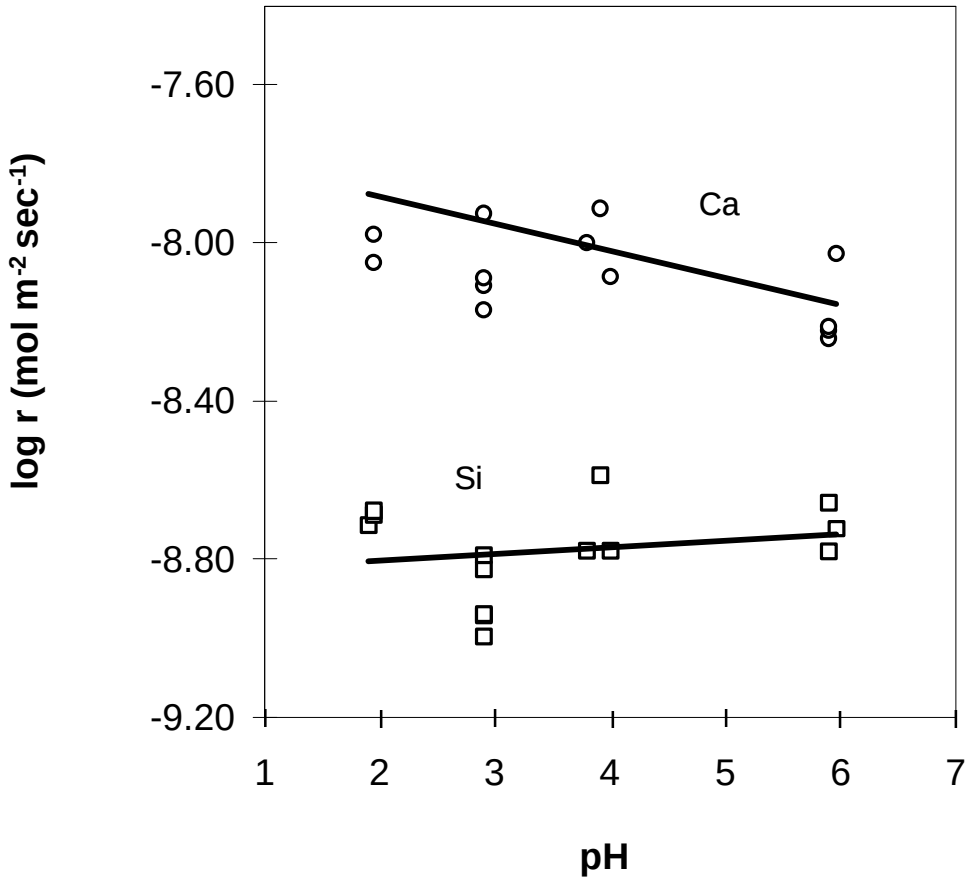

FIG. 4. Comparison of Si and Ca release rates from wollastonite for runs of 25 hour duration, from pH 2 to pH 6. The lines of best fit are y = 0.0168x - 8.837, and y = -0.0684x - 7.7457 for Si and Ca, respectively.

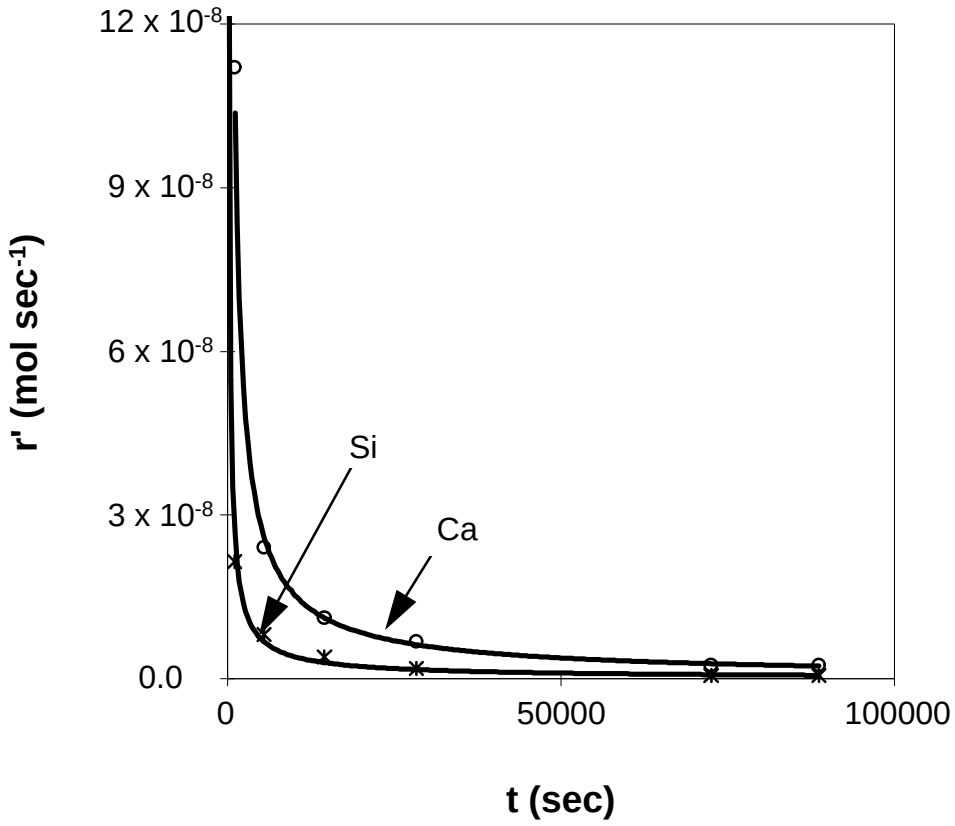

FIG. 5. Apparent release rate curves for Ca and Si from wollastonite over time for run R. These curves are typical of the release rate curves for all the experiments.

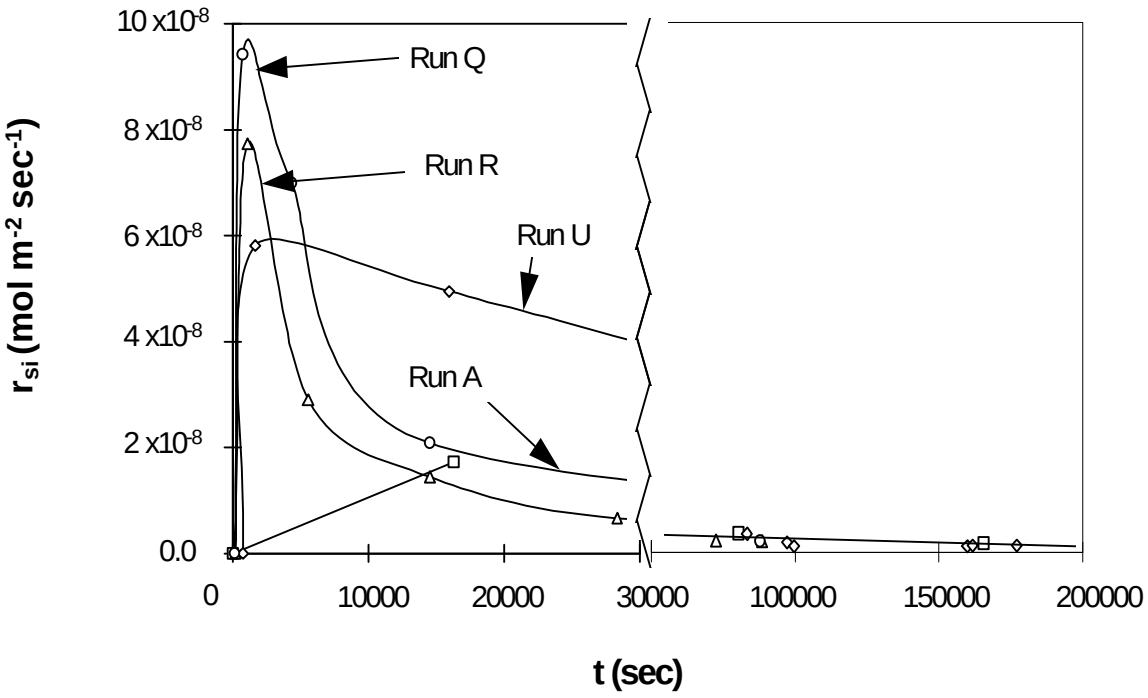

FIG. 6. Comparison of Si release rates for specified runs at pH 2.0. (See Table 1 for run conditions). The time scale has been broken at 30000 sec and been expanded to highlight the differences in initial rates and the similarities in final rates.

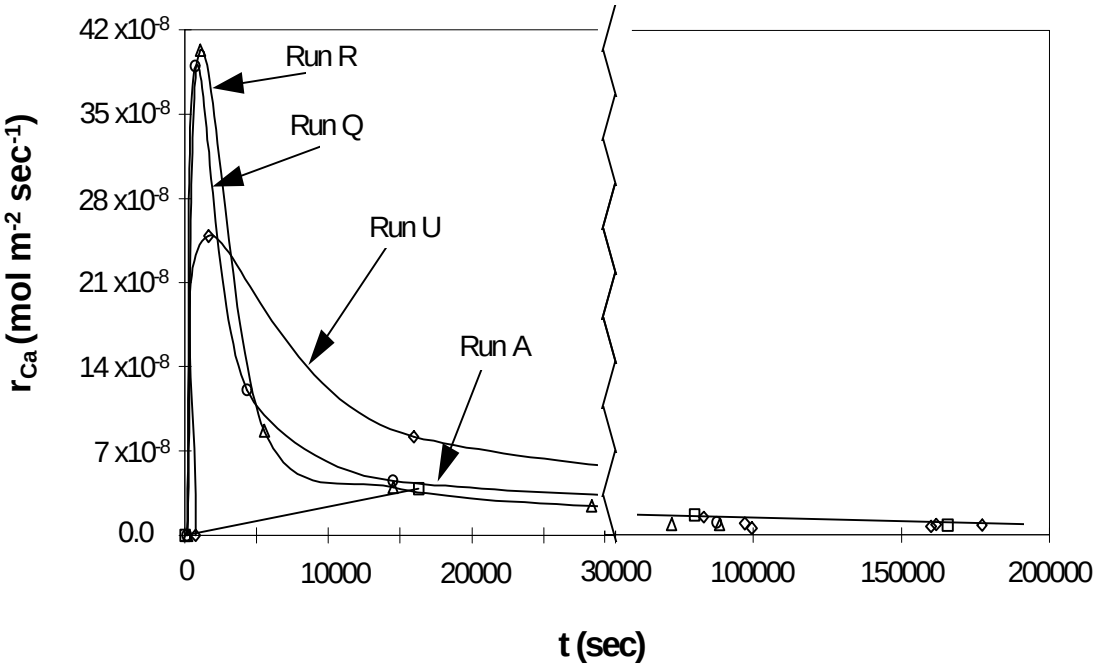

FIG. 7. Comparison of Ca release rates for specified runs at pH 2.0. (See Table 1 for run conditions). The time scale has been broken at 30000 sec and been expanded to highlight the differences in initial rates and the similarities in final rates.

Table 2 shows the averages of the final Ca and Si release rates for all fixed-bed external recycle mixed flow reactor experiments at 25 hours. Because the varying conditions had no influence on the final release rates of Ca or Si, the mean was calculated at each pH using all the experiments. In addition, the mean was calculated for all Si release rates for every experiment over 14 hours to be 2.13×10^{-9} ($\pm 1.03 \times 10^{-9}$ mol/m^2/sec, 1σ, n=67). Within experimental error, the final release rate of Si is independent of pH from pH 2 to 6. The log of the mean Si release rate was submitted to a statistical T test and using a total of 70 data points, there is a 95% probability of being incorrect if the hypothesis that the log r_{Si} equals -8.67 is rejected.

Table 2. Average release rates for experiments up to 25 hours for each pH tested.

pH	Avg. r_{Si} (mol m^{-2} s^{-1})	Avg. r_{Ca} (mol m^{-2} s^{-1})
2	1.80×10^{-9}	9.11×10^{-9}
3	1.29×10^{-9}	8.51×10^{-9}
4	1.97×10^{-9}	10.1×10^{-9}
6	2.06×10^{-9}	8.42×10^{-9}

The Ca release rates in Table 2 appear similar suggesting pH independent release. However, when fitting a line to the data (Fig. 4) the trend is decreasing Ca release with increasing pH. Typically, Ca release rates were 0.7 - 0.8 log units faster than Si release rates in all experiments and log r_{Ca} = -7.75 - 0.07 pH (from Fig. 4). The average r_{Ca} from all experiments over 14 hours is 7.53 x 10^{-9} ($\pm$ 3.88 x 10^{-9} mol/m^2/sec, 1σ, n=42). All of the raw data from every experiment is in Appendix D.

Because Ca release rates were always higher than Si release rates it is assumed there is a uniform thickness, Ca depleted leached layer, formed on the surface of wollastonite. The thickness of this leached layer was calculated using the following equation (Chou and Wollast, 1984):

$$L = \left(\int_1^t (r'_{Ca} - r'_{Si})dt \right) V_m / A \qquad (2)$$

A power function was fit to the Si and Ca release rate data from each experiment and the area between the functions integrated from 60 sec to the end of the experiment. The integration was not begun at t = 0 because of the difficulty in fitting a function from t = 0 to 60 sec; this did not significantly affect the leached layer calculation based on a comparison of integrations begun at 0 and 60 sec. Figure 5 shows a typical fit of the power function to the measured release rates of Ca and Si. When calculating the leached layer thickness, the initial surface area of the solid and molar volumes of both wollastonite and quartz glass were used (Robie et al., 1979). These materials were chosen as possible end member compositions to bracket the probable range of thickness of the leached layer.

Table 3 lists all runs with their final measured BET surface areas, calculated leached layer thickness, and calculated dissolution rates from final specific surface areas. Leached layer thickness could not be calculated for every experiment because either the function was a poor fit or flow conditions were varied in such a way that they disrupted the typical release rate curves. The final surface area for run A could not be measured because of the comminution of the material.

The rates from Table 3 are very different than those calculated using initial A_{sp} because of the very high measured BET surface areas from materials reacted at low pH's. For example, r^*_{si} for run U is two orders of magnitude lower than r_{si} for the same run. In these experiments measured BET surface areas increase from an initial value of 0.3 m^2 g^{-1} to as high as 35 m^2 g^{-1} after less than 100 hours. The lower the initial pH reacting solution the greater the final measured A_{sp}, but also the longer the experiment the greater the final A_{sp}.

A series of experiments was designed and run to show the development of measured BET A_{sp} with time at pH 3. These experiments were run without varying flow rates and unreacted wollastonite was used for each time interval beginning at 1 hour and reacting up to 72 hours. BET surface area was measured for each run and Si release rates calculated normalized with initial A_{sp} (Appendix D, Experiment Hr). A power function was fit to the data (Fig. 8) and suggests that surface area increased quickly and continued to evolve throughout the duration of these experiments.

Table 3. Compilation of final measured BET specific surface areas, the resulting dissolution rates, and the calculated leached layer thicknesses.

Run	pH	A_{sp} ($m^2\ g^{-1}$)	L_{wo} (m)	$L_{qz\ glass}$ (m)	r^*_{Si} (mol $m^{-2}\ s^{-1}$)	r^*_{Ca} (mol $m^{-2}\ s^{-1}$)
A	2.0	NA	1.92×10^{-7}	1.31×10^{-7}	NA	NA
B	4.7	3.70	NA	NA	1.54×10^{-10}	4.60×10^{-10}
D	5.9	5.00	NA	NA	1.00×10^{-10}	3.63×10^{-10}
G	4.0	3.36	2.02×10^{-8}	1.38×10^{-8}	2.53×10^{-10}	12.1×10^{-10}
H	3.9	7.03	4.71×10^{-8}	3.21×10^{-8}	1.10×10^{-10}	5.24×10^{-10}
I	4.0	4.69	3.25×10^{-8}	2.22×10^{-8}	1.07×10^{-10}	5.28×10^{-10}
J	2.9	6.08	4.23×10^{-8}	2.89×10^{-8}	7.00×10^{-11}	5.86×10^{-10}
K	2.9	7.40	4.14×10^{-8}	2.83×10^{-8}	4.16×10^{-11}	3.17×10^{-10}
L	2.9	6.06	5.05×10^{-8}	3.45×10^{-8}	5.68×10^{-11}	4.04×10^{-10}
Hr	2.9	11.13	6.99×10^{-8}	4.77×10^{-8}	3.12×10^{-11}	2.18×10^{-10}
N	5.9	1.69	2.33×10^{-8}	1.59×10^{-8}	3.93×10^{-10}	11.0×10^{-10}
P	6.0	2.23	3.00×10^{-8}	2.05×10^{-8}	2.56×10^{-10}	12.7×10^{-10}
Q	2.0	13.56	9.48×10^{-8}	2.34×10^{-8}	4.57×10^{-11}	2.34×10^{-10}
R	2.0	11.03	8.98×10^{-8}	5.75×10^{-8}	5.75×10^{-11}	2.45×10^{-10}
U	1.9	35.50	1.88×10^{-7}	1.28×10^{-7}	9.61×10^{-12}	0.67×10^{-10}

Leached layers were calculated to be hundreds of Angstroms thick and were thicker for lower pH experiments of the same length (Fig. 9); they range from 230 • at pH 6 to 900 • at pH 2 for experiments up to 24 hours. In experiments conducted for longer durations, up to 200 hours, leached layers were calculated to be close to 2000 • thick. Figure 10 shows that there is a very high correlation between measured BET surface areas and calculated leached layer thickness.

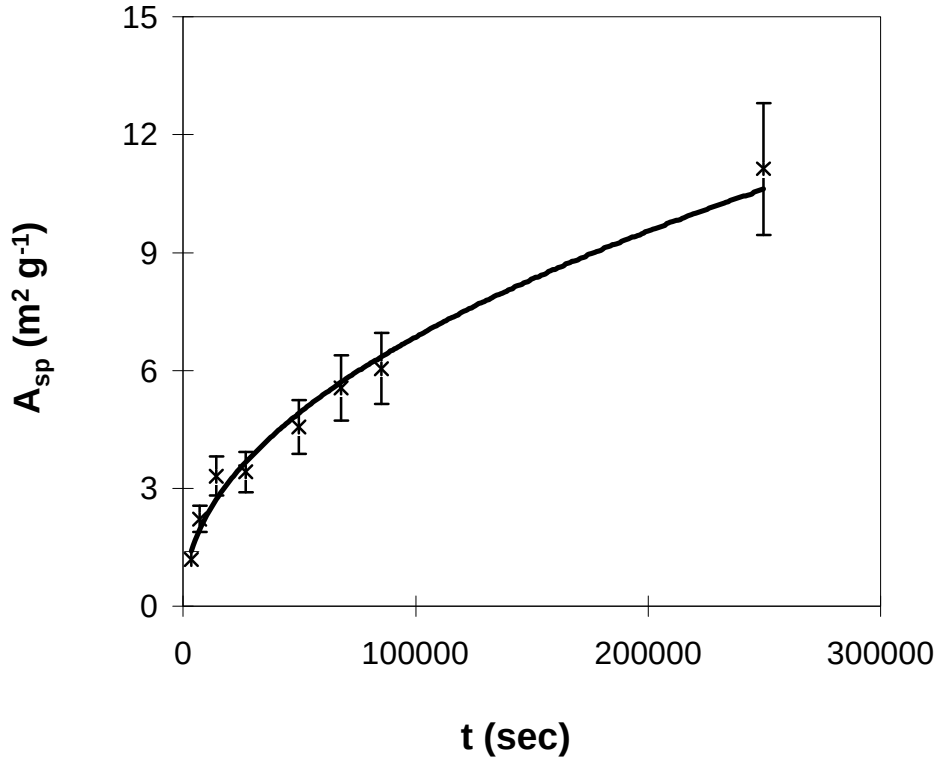

FIG. 8. The results of a series of experiments showing the evolution of BET surface area over time for wollastonite at pH 3.

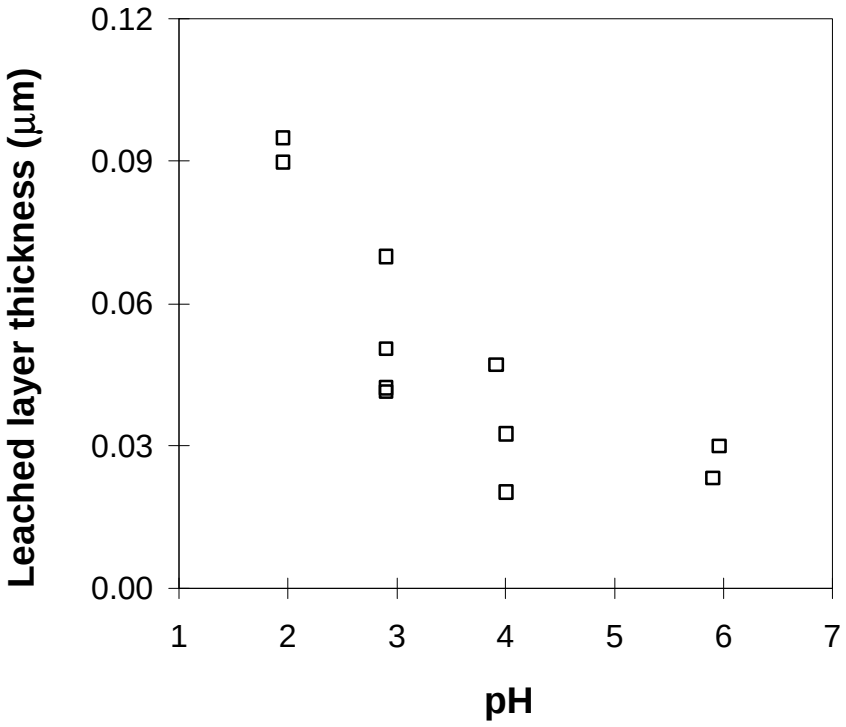

FIG. 9. Calculated leached layer thickness, using the molar volume of wollastonite, versus pH. Although there is scatter in the data due to the narrow range of the y axis, the trend shows a greater thickness of the leached layer at lower pH.

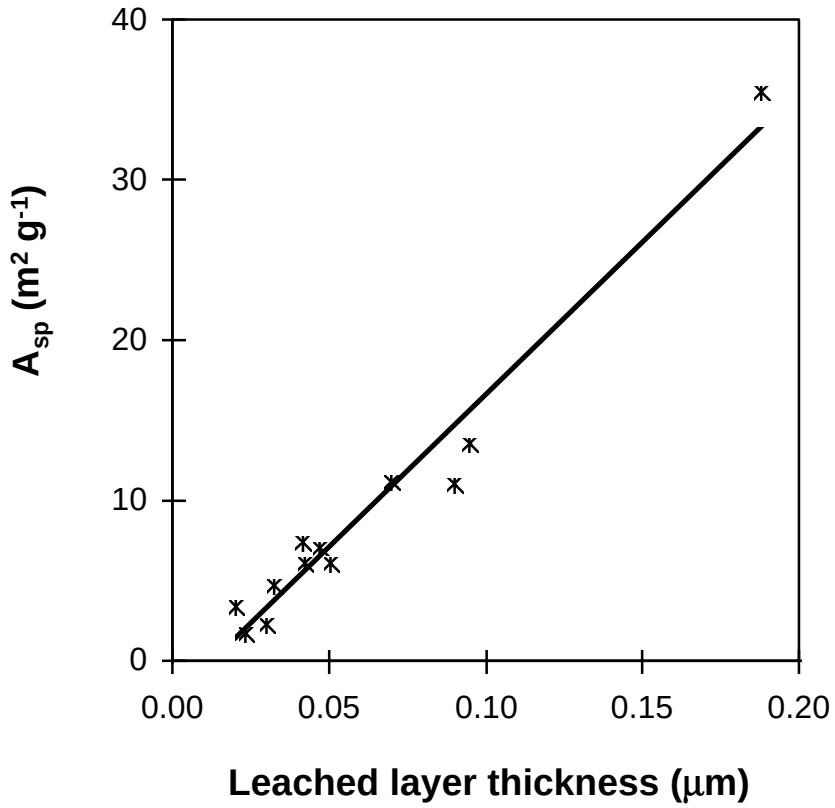

FIG. 10. Comparison of calculated leached layer thickness to measured BET surface area of wollastonite. The plot suggests that the increase in the measured surface area can be attributed to the surface area in the pore spaces of the dehydrated leached layer.

Chapter 7 Discussion

Leached layers often form on the surfaces of silicate minerals that dissolve incongruently. Some previous studies have inferred their existence from nonstoichiometric dissolution rates (e.g., Bailey & Reesman, 1971; Schott et al., 1981; Chou & Wollast, 1984; Schott & Berner, 1985; Xie & Walther, 1994; Stillings & Brantley, 1995) and others have confirmed their existence by direct microscopic examination (e.g., Hochella et al., 1987; Petit et al., 1987; Hellman et al., 1990; Casey et al., 1993; Banfield et al., 1995).

Inosilicates, such as pyroxene, develop a leached layer composed of Si-O chains that remain behind as alkalis and alkaline earths are removed out the crystal. Under acidic conditions, the alkalis and alkaline earths are leached from network aluminosilicates more quickly than aluminum, which hydrolyzes more rapidly than silicon. Hydrogen left behind by the exchange reaction has been measured to depths of hundreds of Angstroms in the remaining leached surface (Petit et al., 1987; Casey et al., 1988). These observations show that it is the hydrolysis of the Si-O bonds in the remaining silica-dominated leached layer that is the rate limiting process in the dissolution of many silicate and aluminosilicate minerals (Muir and Nesbitt, 1991), and not diffusion of metal cations through the leached

layer. At steady state it is believed that the release rates of Si and Ca are coupled; the hydrolysis of the Si-O bonds controls the growth of the leached layer thereby influencing the rate of Ca diffusion through the leached layer.

There is evidence that the Si-enriched surfaces repolymerize to form crosslinked structures (Casey et al., 1988; Casey et al., 1989; Hellman et al., 1990; Casey et al., 1993) by reactions such as:

$$\equiv \text{Si-OH} + \text{HO-Si} \equiv \rightarrow \equiv \text{Si-O-Si} \equiv + H_20$$

Evidence for this comes from the fact that remnant hydrogen measured in the leached layer is less than predicted by the exchange reaction with released Ca^{2+}, Na^{+}, and Al^{3+} (Casey et al., 1988; Casey et al., 1989). Raman spectroscopy of reacted wollastonite shows silica networks that contain four-member rings (Casey et al., 1993). Finally, increasing measured BET surface area has been observed that does not contribute to release rates, suggesting more unreactive surface area. Casey et al. (1993) proposed that the constant or decreasing Si release rates observed as the BET surface area of wollastonite increases, is the result of silica reconstruction in the leached layer into a less reactive form resembling vitreous silica. The increasing BET surface areas coupled with decreasing Si release rates from wollastonite are similar to observations made in our experiments.

It is usually assumed that dissolution rates are directly proportional to a dissolving mineral's surface area (Rimstidt & Barnes, 1980; Lasaga, 1981), but the relationship between dissolution rates and BET surface area does not always follow this trend. Only the portion of the surface area that contains reactive sites contributes to mineral dissolution (Helgelson et al., 1984; Zhang et al., 1993). BET measurements of reacted wollastonite showed large increases in A_{sp} over the course of our experiments, yet the dissolution rate decreased (Fig. 5). Stillings & Brantley (1995) calculated the rate of feldspar dissolution by adjusting their rates to account for this changing surface area. The present experiments show that silica release rates from wollastonite decline as the specific surface area increases from 0.3 to 35.0 m^2g^{-1} (Fig. 11). These large increases of measured A_{sp} are the result of the growing internal porosity of the leached layer (Fig. 1b and Fig. 10). Using final surface areas to calculate dissolution rates treats this leached layer material as if it has the same reactivity as the fresh mineral surface (Brantley & Chen, 1995; Stillings & Brantley, 1995), but this is not consistent with our observation that the release rates of Ca and Si decrease with time. The present study follows the lead of Xie & Walther (1994) who used initial A_{sp} to calculate wollastonite dissolution rates. It follows from these observations of declining Si release rates with time (Fig. 11) that the reactive surface area must be reacting away, leading to a reduction of the density of reactive, high-energy surface sites (White et al., 1996). It has already been demonstrated that much of the final wollastonite A_{sp} is due to internal surface area (Fig. 10), and this surface does not seem to contribute to Si release rates.

From the initial incongruent dissolution of wollastonite it can be inferred that the initial dissolution processes of Ca and Si from wollastonite are independent of each other. This

suggests that rate laws that are based on reaction affinity (Lasaga, 1995) should not apply to these incongruent reactions. The independent reactivity of wollastonite components is consistent with the additivity model of silicate thermodynamics (Chermak & Rimstidt, 1989) that models the ΔG_f^o and ΔH_f^o of minerals as if they are made up of a collection of independent oxide polyhedra. A higher concentration of Ca in the reactor effluent was always observed, suggesting that Si is being left behind as part of a leached layer on the mineral surface; this is consistent with the lower solubility of SiO_2 compared to CaO. The existence of the Si-enriched leached layer was confirmed by qualitative EDX analysis of unreacted and reacted grains. A comparison of the Si/Ca peak ratios showed the ratio changed from 0.87 to 2.87 respectively (Appendix B) and SEM photographs of reacted wollastonite surface (Fig. 1b) verify the existence of the leached layer. Thus the overall reaction for the hydrolysis of wollastonite in an acid environment is best explained by a two step process (Murphy & Helgeson, 1987):

$$nCaSiO_3 + 2nH^+ \rightarrow nCa^{2+} + (H_2SiO_3)_n \quad (3)$$

$$(H_2SiO_3)_n + nH_2O \rightarrow n(H_4SiO_4) \quad (4)$$

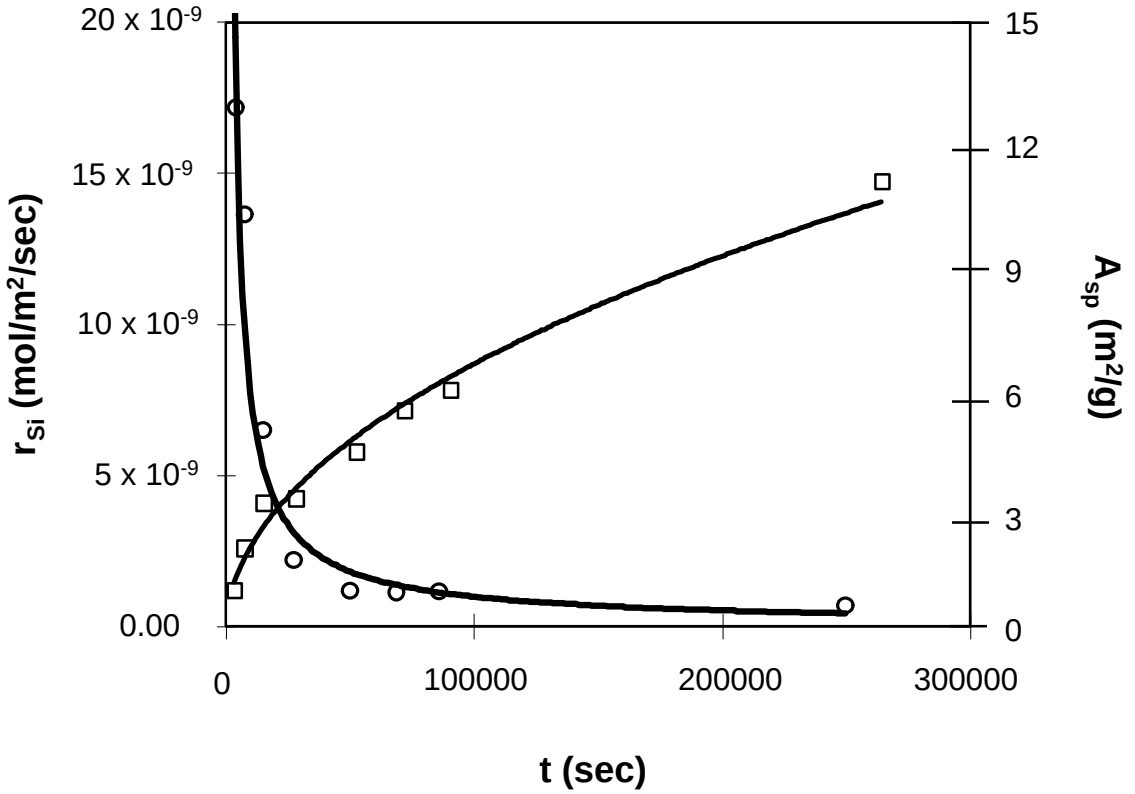

FIG. 11. Plot of Si release rate versus time for experiment Hr. This experiment showed the evolution of BET surface area by measuring A_{sp} at each time interval. It is clearly shown how the Si rate decreases with time despite increasing BET A_{sp}.

If the hydrolysis of Si at the wollastonite surface formed a silica gel with the approximate composition $(H_2SiO_3)_n$, perhaps the dissolution rate of this Si could be predicted from our knowledge of SiO_2 dissolution rates (Rimstidt and Barnes, 1980). According to the principle of detailed balancing, the equilibrium constant (*K*) for a reaction is equal to the forward reaction rate constant (k_+) divided by the reverse reaction rate constant (k_-), or

$$K = k_+ / k_- \quad (5)$$

Rimstidt and Barnes (1980) showed that k_- is the same for all silica phases. Therefore if *K* can be estimated, we can predict k_+ for near equilibrium conditions. If the leached layer had a solubility equivalent to highly polymerized amorphous silica, or silica glass, log *K* would be -11.89 and log $k_{+\,(amsil)}$ would equal -12.13, so $r = 10^{-12.13}$ mol/m^2/s. This calculated rate is three and a half orders lower than the measured r_{si} of wollastonite, $r_{si(wo)} = 10^{-8.67}$ mol/m^2/sec, suggesting that the leached layer is not highly polymerized. The calculated rate would be higher for a more soluble hydrated silica polymer, $(H_2SiO_3)_n$. We can estimate the ΔG_f^o, and the solubility of this hydrated silica using an additivity model as follows:

$$H_2SiO_3 = \frac{1}{2} SiO_{2\,(am)} + \frac{1}{2} H_4SiO_4 \text{ , so} \quad (6)$$

$$\Delta G_{f\,(H2SiO3)}^o = \frac{1}{2} \Delta G_{r\,(SiO2(am))}^o + \frac{1}{2} \Delta G_{r\,(H4SiO4)}^o \quad (7)$$

$$\Delta G_{f\,(H2SiO3)}^o = \frac{1}{2}(-853.95) + \frac{1}{2}(-1308) \quad (8)$$

The values of -853.95 and -1308 kJ/mol are from Chermak and Rimstidt (1989), and Robie et al., (1979) respectively.

$$= -1080.975 \text{ kJ/mol}$$

$$\Delta G_r^o = -1{,}308 - (-1{,}080.975) - (-237.141) \quad (9)$$

$$\Delta G_r^o = 10.12 \text{ kJ/mol}$$

$$\log K = -10116/(2.303\ RT) \quad (10)$$

$$\log K = -1.77$$

$$K = 10^{-1.77}$$

Following the same procedure as above to calculate k_+:

$$k_+ = (10^{-1.77})(10^{-9.42}) = 10^{-11.19} \quad (11)$$

$$r = 10^{-11.19} \text{ mol/m}^2\text{/s} \quad (12)$$

This is still two and a half orders of magnitude lower than the observed rate of Si release from wollastonite suggesting that the leached layer dissolution reaction occurs so far from equilibrium that the principle of detailed balancing fails to apply. This failure probably arises because the reaction mechanism at steady state is different than for the near

equilibrium conditions where only monomeric silica is released by Si-O-Si bond hydrolysis. However, the observed high rate of Si release could perhaps be explained if the leached layer consisted of silica chains remaining from the wollastonite structure and the hydrolysis of Si-O-Si bonds at various places along these chains releases polymers of various lengths into solution (Fig. 12). As these polymers are released into solution they quickly break down to monomers yielding the high measured Si release rates for wollastonite.

The Ca release rate was very high at the beginning of each of our experiments and the rate declined over time in a way that suggests that it will eventually become equal to the Si release rate. Thus, the reaction seems to evolve from very nonstoichiometric dissolution that rapidly produces leached-layer silica to one that becomes more or less stoichiometric so that leached-layer silica is produced at the same rate as it dissolves. This behavior can be easily explained if the rate of Ca release is controlled by its transport through the leached layer.

Equation (3) suggests that Ca removal from wollastonite should be much faster at low pH. This means that leached layer silica is produced faster at low pH as is shown in Fig. 9. However, the dissolution rate of the silica in the leached layer is independent of pH (equation 4, and Fig. 4). This means that the leached layer is thicker at low pH (Fig. 9) and presents a longer diffusion path for Ca transport into the solution. This offsets the faster rate of reaction (3) so that at steady state the Ca rates should also become pH independent.

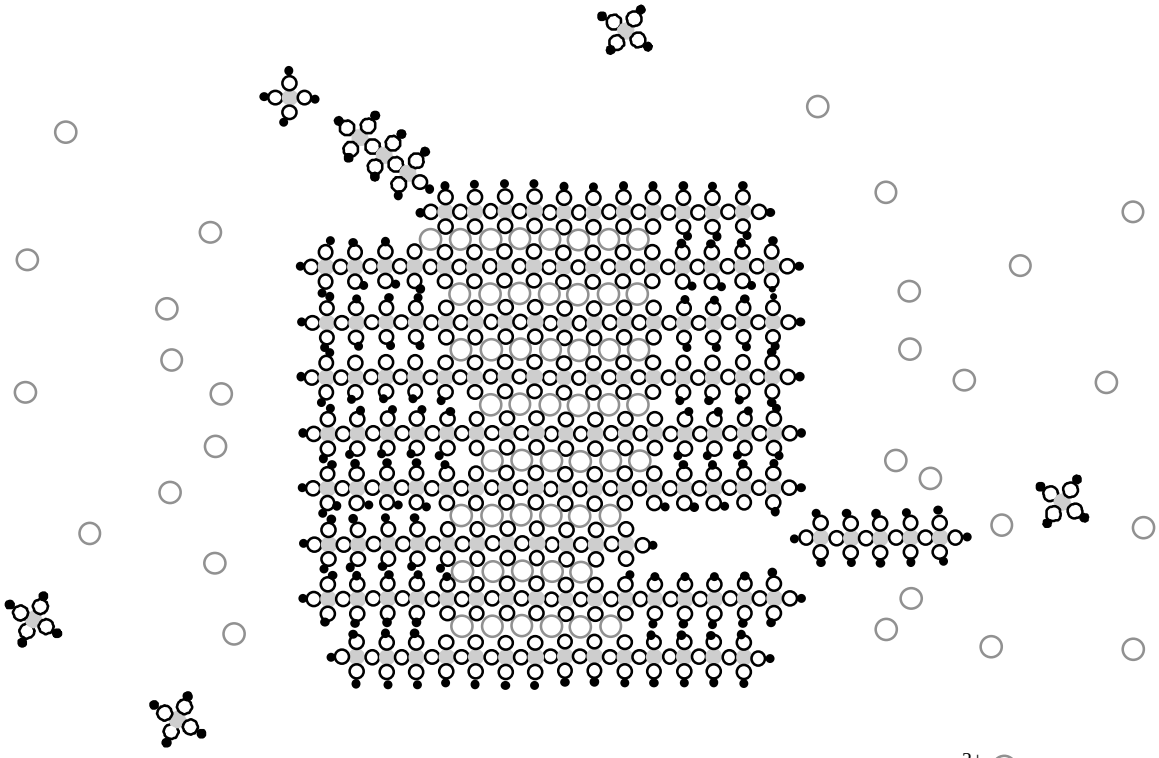

FIG. 12. Schematic representation of proposed wollastonite dissolution. Ca^{2+} ○ diffuses through the Si ● enriched leached layer. The rate of Ca^{2+} dissolution is dependent upon

the thickness of the leached layer that is dependent upon the H^+ • concentration. The hydrolysis of Si is related to polymer dissolution.

Previously we have shown how to calculate the thickness of the leached layer using equation (2). Taking this step further it is possible to model the rate of the leached layer growth (dx) with time (dt):

$$\frac{dx}{dt} = (r_{Ca}\text{-}r_{Si})V_m \qquad (13)$$

Transport through the leached layer is modeled as diffusion through a layer of thickness x (Muir & Nesbitt, 1997):

$$r_{Ca} = \frac{D}{10\Delta x}(m_{Ca,\,xtl} - m_{Ca,\,sfc}) \qquad (14)$$

Where D is the diffusion coefficient in (cm^2/s) and ($m_{Ca,\,xtl} - m_{Ca,\,sfc}$) is the change in concentration of Ca from the wollastonite/leached layer interface to the leached layer/solution interface or Δm_{Ca} in (mol/L) (Fig. 13). Substituting (14) into (13) we have:

$$\frac{dx}{dt} = (\frac{D}{\Delta x}(\Delta m_{Ca}) - r_{Si})Vm/10) \qquad (15)$$

At steady state the leached layer growth rate is zero, hence the thickness of the steady state leached layer:

$$x_{ss} = D\,\Delta m_{Ca} / 10\, r_{Si} \qquad (16)$$

Equation (16) shows that the leached layer thickness is proportional to the change in Ca concentration. This difference should be greatest at low pH supporting our observation that the greatest leached layer thickness occurs at low pH.

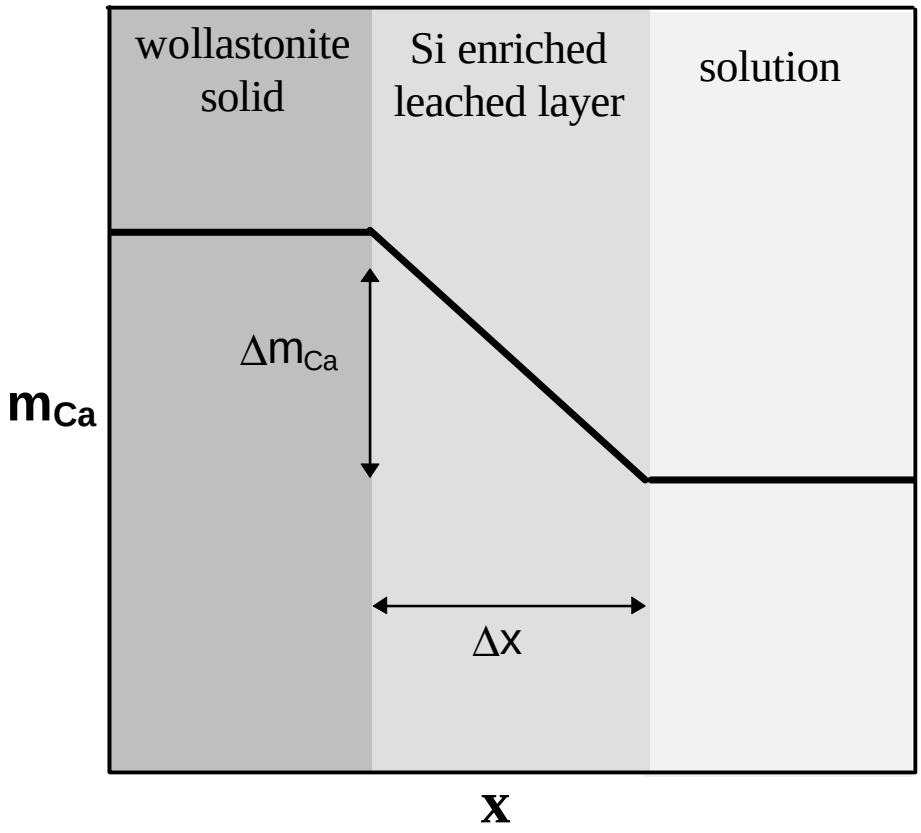

FIG. 13. Schematic representation of the wollastonite surface. Diffusion of Ca^{2+} through the Si enriched layer is dependent on the change in concentration of Ca from the solid to the solution (Δm_{Ca}) and the thickness of the leached layer (Δx).

Chapter 8 Conclusions

A new reactor was designed to investigate the dissolution rate of wollastonite. This design was necessary to overcome comminution effects and transport limited dissolution. A comprehensive series of experiments was run from pH 2 through pH 6 varying operating conditions to test the effect of changes on Ca and Si release rates (Table 1). A comparison of the results with previous work (Fig 14) shows that the Si release rate data is in the same range; however the results of this study have shown that the Si release rate is independent of pH (Fig. 4).

There are a few important issues that arise from observations made while conducting these experiments. By varying flow conditions, it was possible to affect initial Ca and Si release rates from wollastonite, but final, near steady state release rates, were independent of the flow conditions used in this study(Figs. 6 & 7). The dissolution of wollastonite was nonstoichiometric up to 190 hours with Ca dissolving at a faster rate than Si, but the Ca release rate approached the Si release rate over the course of the experiments suggesting that the reaction will eventually become congruent (Fig. 5). The initial incongruent dissolution of wollastonite leads to the formation of a leached layer on the surface of

wollastonite. The cracked and porous nature of the dehydrated leached layer was the cause of the large BET surface area increases measured on wollastonite (Fig. 10); however the leached layer thickness apparently had no affect on final Si release rates.

It is proposed that the dissolution of wollastonite is a two-step process. Ca is released from wollastonite at a rate that depends on the pH of the solution. The rapid initial Ca release leads to the formation of a Si-enriched leached layer composed of hydrated silica. As the leached layer thickness increases, the Ca release rate slows measurably because the Ca has to diffuse through the leached layer to enter the solution. Ultimately, the Ca release rate appears to become equal to the Si release rate, which is independent of pH (Fig. 4). This occurs because the leached layer is thicker at low pH (Fig. 9) and it is this thickness that controls the rate of Ca release (Fig. 13).

It is the hydrolysis of Si that is the overall rate controlling step in the dissolution of wollastonite. Under acidic conditions, the hydrolysis rate of Si-O-Si is independent of pH and this rate controls the thickness of the leached layer. The rate of Si release from wollastonite is much faster than that predicted from the principle of detailed balancing. We propose that the fast release of Si from wollastonite is due to the hydrolysis of Si-O-Si bonds at random sites along the hydrated silica chains so that linear silica polymers are released into the solution, these polymers subsequently hydrolyze to silica monomers (Fig. 12). This theory agrees well with those that propose repolymerization of the Si-O chains (Casey et al., 1988; Casey et al., 1989; Hellman et al., 1990; Casey et al., 1993) and explains the high rate of Si release from wollastonite.

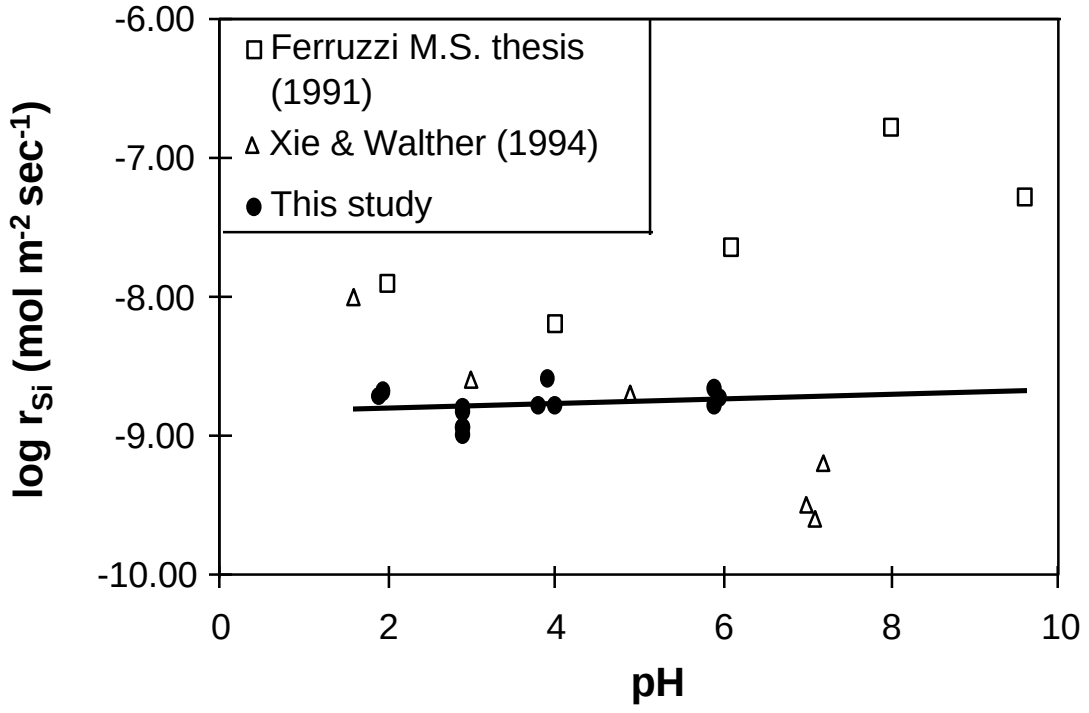

FIG. 14. Comparison of log Si release rates from wollastonite reported by various studies.

References

Bailey A. and Reesman A. L. (1971) A survey study of the kinetics of wollastonite dissolution in H_2O and buffered systems at 25°C. *Amer. J. Sci*. **271**, 464-472.

Banfield J. F. and Barker W. W. (1994) Direct observation of reactant-product interfaces formed in natural weathering of exsolved, defective amphibole to smectite: Evidence for episodic, isovolumetric reactions involving structural inheritance. *Geochim. Cosmochim. Acta* **55**, 1419-1429.

Banfield J. F., Ferruzzi G. G., Casey W. H., and Westrich H. R. (1995) HRTEM study comparing naturally and experimentally weathered pyroxenoids. *Geochim. Cosmochim. Acta***. 59**, 19-31.

Brantley S. L. and Chen Y. (1995) Chemical weathering rates of pyroxenes and amphiboles. In *Chemical Weathering Rates of Silicate Minerals* (A. F. White and S. L. Brantley, Eds.) 31,120-172. Mineralogical Society of America.

Brunauer S., Emmet P. S., and Teller E. (1938) Adsorption of gases in multimolecular layers. *J. Amer. Chem. Soc.* **60**, 309-319.

Casey W. H., Westrich H. R., and Arnold G. W. (1988) Surface chemistry of labradorite feldspar reacted with aqueous solutions at pH = 2, 3, and 12. *Geochim. Cosmochim. Acta***. 52**, 2795-2807.

Casey W. H., Westrich H. R., Arnold G. W., and Banfield J. F. (1989) The surface chemistry of dissolving labradorite feldspar. *Geochim. Cosmochim. Acta***. 53**, 821-832.

Casey W. H., Westrich H. R., Banfield J. F., Ferruzzi G., and Arnold G. W., (1993) Leaching and reconstruction at the surfaces of dissolving chain-silicate minerals. *Nature* **366**, 253-256.

Chou L. and Wollast R. (1984) Study of the weathering of albite at room temperature and pressure with a fluidized bed reactor. *Geochim. Cosmochim. Acta* **48**, 2205-2217.

Chermak J. A. and Rimstidt J. D. (1989) Estimating the thermodynamic properties (ΔG_f^o and ΔH_f^o) of silicate minerals at 298 K from the sum of polyhedral contributions. *American Mineralogist* **74**, 1023-1031.

Ferruzzi G. G. (1994) *The character and rates of dissolution of pyroxenes and pyroxenoids.* unpubl. M.Sc. thesis, Univ. California Davis.

Helgeson H. C., Murphy W. M. and Aagaard P. (1984) Thermodynamic and kinetic constraints on reaction rates among minerals and aqueous solutions. II. Rate constants, effective surface area, and hydrolysis of feldspar. *Geochim. Cosmochim. Acta* **48**, 2405-2432.

Hellman R., Eggleston C. M., Hochella M. F., and Crerar D. A. (1990) The formation of leached layers on albite surfaces during dissolution under hydrothermal conditions. *Geochim. Cosmochim. Acta.* **54**, 1267-1281.

Hochella M. F., Ponader H. B., Turner A. M., and Harris D. W. (1988) The complexity of mineral dissolution as viewed by high resolution scanning Auger microscopy: labradorite under hydrothermal conditions. *Geochim. Cosmochim. Acta.* **52**, 385-394.

Lasaga A. C. (1981) Kinetics of geochemical processes. In *Reviews in Mineralogy* (A. C. Lasaga and R. J. Kirkpatrick, Eds.) 8, 1-67. Mineralogical Society of America.

Lasaga A. C. (1995) Fundamental approaches in describing mineral dissolution and precipitation rates. In *Chemical Weathering Rates of Silicate Minerals* (A. F. White and S. L. Brantley, Eds.) 31, 23-86. Mineralogical Society of America.

Muir I. J. and Nesbitt H. W. (1991) Effects of aqueous cations on the dissolution of labradorite feldspar. *Geochim. Cosmochim. Acta.* **55**, 3181-3189.

Muir I. J. and Nesbitt H. W. (1997) Reactions of aqueous anions and cations at the labradorite-water interface: coupled effects of surface processes and diffusion. *Geochim. Cosmochim. Acta.* **61**, 265-274.

Murphy W. M. and Helgeson H. C. (1987) Thermodynamic and kinetic constraints on reaction rates among minerals and aqueous solutions. III. Activated complexes and the pH-dependence of the rates of feldspar, pyroxene, wollastonite, and olivine hydrolysis. *Geochim. Cosmochim. Acta* **51**, 3137-3153.

Petit J-C., Della Mea G., Dyan J-C., Schott J., and Berner R. A. (1987) Mechanism of diopside dissolution from hydrogen depth profiling. *Nature* **325**, 705-707.

Rimstidt J. D. and Barnes H. L. (1980) The kinetics of silica-water reactions. *Geochim. Cosmochim. Acta.* **44**, 1683-1699.

Rimstidt J. D. and Dove P. M. (1986) Mineral/solution reaction rates in a mixed flow reactor: wollastonite hydrolysis. *Geochim. Cosmochim. Acta* **50**, 2509-2516.

Rimstidt J. D. and Newcomb W. D. (1993) Measurement and analysis of rate data: The rate of reaction of ferric iron with pyrite. *Geochim. Cosmochim. Acta* **57**, 1919-1934.

Robie R. A., Hemingway B. S., and Fisher J. R. (1979) Thermodynamic properties of minerals and related substances at 298.15 K and 1 bar (10^5) pressure and at higher temperature. *USGS Bull.* **1452**.

Schott J., Berner R. A., and Sj″berg E. L. (1981) Mechanism of pyroxene and amphibole weathering-I. Experimental studies of iron-free minerals. *Geochim. Cosmochim. Acta* **45**, 2123-2135.

Stillings L. L. and Brantley S. L. (1995) Feldspar dissolution at 25oC and pH 3: Reaction stoichiometry and the effect of cations. *Geochim. Cosmochim. Acta* **59**, 1483-1496.

Taylor J. R. (1982) *An Introduction to Error Analysis: The Study of Uncertainties in Physical Measurements.* University Science Books, Mill Valley, California. 270p.

White A. F., Blum A. E., Schulz M. S., Bullen T. D., Harden J. W., and Peterson M. L. (1996) Chemical weathering rates of a soil chronosequence on granitic alluvium: I. Quantification of mineralogical and surface area changes and calculation of primary silicate reaction rates. *Geochim. Cosmochim. Acta* **60**, 2533-2550.

Xie Z. and Walther J. V. (1994) Dissolution stoichiometry and adsorption of alkali and alkaline earth elements to the acid-reacted wollastonite surface at 25°C. *Geochim. Cosmochim. Acta* **58**, 2587-2598.

Zhang H., Bloom P. R., and Nater E. A. (1993) Change in surface area and dissolution rates during hornblende dissolution at pH 4.0. *Geochim. Cosmochim. Acta* **57**, 1681-1689.

APPENDIX A Nomenclature

A	total surface area of the solid (m^2)
Asp	specific surface area of the solid ($m^2\ g^{-1}$)
D	diffusion coefficient (m/s)
ΔG_f^o	free energy of formation (kJ mol^{-1})
ΔG_r^o	free energy of reaction (kJ mol^{-1})
K	equilibrium constant
$L_{qz\ glass}$	leached layer thickness calculated using the molar volume of quartz glass (m)
L_{wo}	leached layer thickness calculated using the molar volume of wollastonite (m)
M	mass of solution (g)
R	gas constant (8.318 J mol^{-1} K^{-1})
T	temperature (K)
V_m	molar volume of the solid (m^3 mol^{-1})
k_+	dissolution rate constant (sec^{-1})
k_-	precipitation rate constant (sec^{-1})
Δm_{Ca}	net concentration change of Ca from the wollastonite/leached layer interface to the leached layer/solution interface (mol/m^2)
r_{Si}	release rate of silica (mol m^{-2} sec^{-1})
r_{Ca}	release rate of calcium (mol m^{-2} sec^{-1})
r^*_{Si}	release rate of silica calculated from final surface area (mol m^{-2} sec^{-1})
r^*_{Ca}	release rate of calcium calculated from final surface area (mol m^{-2} sec^{-1})
r'_{Si}	apparent rate of silica release from solid (mol sec^{-1})
r'_{Ca}	apparent rate of calcium release from solid (mol sec^{-1})
m_j	concentration of component j (mol)
r_c	recycle rate of solution in the reactor (L sec^{-1})
r_f	solution flow rate through the reactor (L sec^{-1})
r_j	release rate of component j (mol m^{-2} sec^{-1})
t	time (sec)
x	leached layer thickness (m)